Advanced Materials

ADVANCED MATERIALS
www.advmat.de

RESEARCH ARTICLE OPEN ACCESS

Transparent Perovskite Light-Emitting Diodes with Conductive Oxide Top Electrodes

Michele Forzatti[1] | Sergio Martínez-Saiz[1] | Morena Cervino[1] | Edoardo Stanzani[2] | Sandra Jenatsch[2] | Qingsen Zeng[3] | Joo Sung Kim[3] | Dong-Hyeok Kim[3] | Eojin Yoon[3] | Tae-Woo Lee[3,4] | Daniel Tordera[1] | Henk J. Bolink[1]

[1]Institute of Molecular Science, University of Valencia, Paterna, Spain | [2]FLUXiM AG, Winterthur, Switzerland | [3]Department of Materials Science and Engineering Research Institute of Advanced Materials, Seoul National University, Seoul, Republic of Korea | [4]Institute of Engineering Research, Soft Foundry, Interdisciplinary Program in Bioengineering, Seoul National University, Seoul, Republic of Korea

Correspondence: Tae-Woo Lee (twlees@snu.ac.kr) | Daniel Tordera (daniel.tordera@uv.es) | Henk J. Bolink (henk.bolink@uv.es)

Received: 2 November 2025 | **Revised:** 21 February 2026 | **Accepted:** 27 February 2026

Keywords: in situ perovskite nanocrystals | perovskite light-emitting diodes | pulsed laser deposition | transparent light-emitting diodes | transparent oxide electrodes

ABSTRACT

Transparent light-emitting diodes (TrLEDs) allow to simultaneous display data while maintaining the visibility of the surroundings. This feature unlocks a new range of applications. Perovskite-based emitting materials are promising for such devices in view of their narrow emission spectrum and color tunability. Here, we show that depositing an indium tin oxide (ITO) electrode using pulsed laser deposition in combination with a metal oxide buffer layer is a universal approach for the fabrication of transparent perovskite LEDs (TrPeLEDs) with a variety of compositions and device configurations. Green TrPeLEDs based on in situ formed perovskite nanocrystals (NC) deposited directly on ITO coated glass substrates achieved a record-high combined luminance of 150 000 cd m^{-2}. When instead a TrPeLED using a thin colloidal NCs layer was used it led to LEDs with an average visible transmittance of 80% and a color rendering index above 90.

1 | Introduction

Molecular semiconductors are used on a wide scale in organic light-emitting diodes (OLEDs). In these OLEDs the emitters can be purely of an organic nature but frequently also contain organometallic complexes as the primary emitter. Notable examples are phosphorescent iridium complexes. Metal halide perovskites (MHPs) have also been employed as emitters in OLEDs. The first demonstrations of MHP-based LEDs date back to 1992, when Hong et al. reported electroluminescence from lead iodide–based quantum well structures below 200 K [1]. In 1999, Chondroudis and Mitzi achieved room-temperature electroluminescence from organic–inorganic perovskites through the incorporation of an organic dye cation into the perovskite structure [2]. The use of MHP emitters in OLEDs re-emerged in 2014, with electroluminescence demonstrated in the near-infrared, green, and red regions by tuning the halide composition, achieving external quantum efficiencies of up to 0.76% [3, 4]. Since then, perovskite LEDs (PeLEDs) have achieved electroluminescence external quantum efficiencies (EQEs) exceeding 30% for near-infrared, red, and green emission, and above 26% for blue perovskite LEDs [5–8]. MHPs have also been used as charge transport layers in LEDs using molecular emitters [9–15]. In all these examples, the LEDs have a similar thin film structure as OLEDs and they employ organic semiconductors. These MHP containing LEDs can therefore be considered as a subclass of

We dedicate this article to Prof. Paul Blom, for his outstanding contributions on the advancements of organic electronic devices, on the occasion of his 60th Birthday.

thin film LEDs. And just like organic semiconductors, MHPs can be processed into thin films by sublimation or solvent-based methods.

MHPs have the general ABX_3 formula in which A is usually an alkyl-ammonium cation, B is the lead cation, and X a halide anion. These materials have found interest in many optoelectronic applications due to their attractive properties, such as facile synthesis, strong optical absorption, high conductivity, and large exciton diffusion lengths [14, 16–18]. Moreover, their properties can be modified by selecting the A and B cations as well as the halide anion [19]. This vast compositional flexibility has enabled the fine tuning of the emission wavelength and efficiency.

The narrow emission spectra and high luminescence efficiencies of MHPs make them ideal emitters for LEDs [20, 21]. The compositional flexibility of perovskites is beneficial because it allows to tune their emission wavelength. PeLEDs can be made of polycrystalline 3D and quasi-2D MHPs that have relatively large crystal grains [4, 22]. Alternatively, PeLEDs can also be prepared using colloidally synthesized perovskite nanocrystals (NCs) [23–25]. In these NC, the exciton binding energy is enhanced due to the stronger carrier confinement. Yet this benefit comes at the cost of a decrease in charge injection and transport capabilities caused by the insulating long-chain ligands. Recently, the in situ-formation of NCs domains in a 3D perovskite films was reported [26]. This was achieved by adding small amounts of benzylphosphonic acid (BPA) to the perovskite precursor solution, which during the film formation leads to the formation of discrete crystals end-capped with the BPA molecules. The resulting films had improved exciton binding energy and radiative recombination efficiency while maintaining good charge injection and transport properties. Other molecular dopants containing phosphonic acid groups are also able to constrain the growth of perovskite crystals during film formation [27, 28]. Furthermore, phosphonic acid molecular dopants with strong electron-withdrawing abilities are also able to induce a transition from n-type to p-type conductivity in the perovskite, which is beneficial as it allows for a greatly simplified, hole-transport layer (HTL)-free device architecture with efficient carrier injection [28].

Transparent light-emitting diodes (TrLEDs) allow the preparation of full-color flat panel displays by vertical device stacking [29]. Moreover, TrLED can also be integrated into building facades, windows, head-up panels in cars or in smart wearables [30]. TrLEDs use transparent electrodes at both terminals, and thus light can exit in both directions. Most thin film LEDs use transparent conductive oxides (TCOs) such as Indium Tin Oxide (ITO) as the bottom electrode [29]. However, it is very challenging to deposit these TCOs on top of the fragile thin film structure of perovskite LEDs. TCO are usually deposited by sputtering or pulsed laser deposition generating TCO fragments with high kinetic energy, which can damage the underlaying device stack. Furthermore, to achieve high quality TCO's a high temperature annealing is often required. For these reasons, perovskite-based TrLEDs have so far used semi-transparent electrodes based on thin metal stacks. In one example, a 3D film of $MAPbBr_3$ was used as the emissive layer (EML) and a $LiF/Al/Ag/MoO_3$ (dielectric–metal–dielectric, DMD) multilayer was employed as the transparent top electrode [31]. In recent reports, these TrLEDs using DMD transparent electrodes had moderate efficiencies and average transmittance [32–39].

In this report, we describe the development of very efficient perovskite LEDs using different EML approaches and we develop a universal method to deposit ITO electrodes on top of the perovskite-based LED stacks. Using an EML with in situ-formed nano-crystalline domains we obtain efficient (EQE of 11%) green emitting perovskite LEDs reaching very high luminance levels of 150 000 cd m^{-2} while maintaining an average visible transmittance of 53%. We assessed the devices' aesthetic properties and describe the key factors that allow for the fine turning of the performance and transparency. Finally, we demonstrated the universality of our TCO deposition approach by applying it to LEDs employing an EML consisting of colloidal nanoparticle-based perovskites. In these more transparent LED stacks an average visible transmittance of 80% was achieved with a color rendering index (CRI) above 90.

2 | Results and Discussion

2.1 | Universal Approach for the Deposition of TCO's on PeLED Structures

The first PeLED structure we focused on employs an EML consisting of in situ formed nano-crystalline domains of (4-(9H-carbazol-9-yl)butyl)phosphonic acid (4PACz)-containing $(FA_{0.8}MA_{0.1}GA_{0.1})_{0.87}Cs_{0.13}PbBr_3$ (hereafter, p-type in situ NCs) [28]. An average size distribution of the perovskite NCs of 109.08 ± 45.49 nm was determined via SEM imaging (Figure S1). The valence band maximum (5.79 eV) and conduction band minimum (3.56 eV) was derived from the photoemission spectrum and the tauc plot obtained from the absorption spectrum (Figure S2). This EML (150 nm) was deposited directly on the ITO coated glass substrates and covered with a thin (20 nm) layer of 2,4,6-tris[3-(diphenylphosphinyl)phenyl]-1,3,5-triazine (PO-T2T). PO-T2T served as electron-transport layer (ETL). The perovskite layer was deposited directly on top of ITO, thanks to the doping of 4PACz in the perovskite, which eliminates the need for HTLs [28]. To alleviate potential sputter damage during ITO deposition the stack was finished by a thin layer (20 nm) of SnO_x deposited using atomic layer deposition (ALD). SnO_x was used because its conduction band lies in between that of ITO and the lowest unoccupied molecular orbital (LUMO) of PO-T2T (energy level diagram in Figure S3). Additionally, its wide bandgap ensures a high optical transmission and broadband transparency (detailed transmittance spectrum in Figure 4a). Its high carrier concentration and conductivity will aid the charge injection and reduce injection voltages, and the matching refractive index with the adjacent ITO layer reduces reflection losses [40]. For clarity, devices with this architecture will be referred to as "***1a***". A schematic of this device stack (including the top ITO electrode) is depicted in Figure 1a. The thicknesses of all the layers were confirmed with scanning electron microscopy (Figure S4).

As a first approach, DC magnetron sputtering was used to deposit the ITO [41]. Thin Ag gridlines were positioned outside the pixel area to reduce the sheet resistance of the top electrode. To confirm the protective role of the SnO_x layer, devices without it were

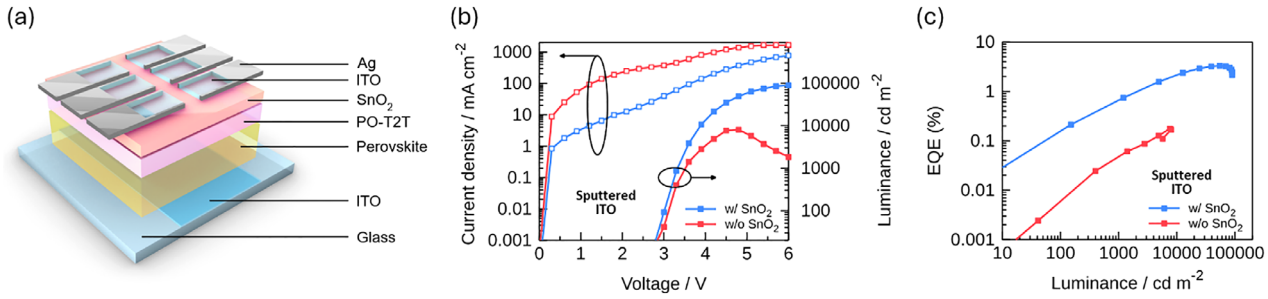

FIGURE 1 | TrPeLEDs based on p-type in situ NCs and with a sputtered ITO cathode. (a) Schematic representation of the devices' structure (devices "*1a*"). (b) Current density and luminance *vs* voltage curves (devices "*1a*" and "*1b*"). (c) Efficiency *vs* luminance plot for the same devices. The reported data refers to the combined top and bottom emission.

also fabricated (devices "***1b***"). The current density versus voltage curves of these two types of stacks are displayed in Figure 1b. The current density rises rapidly when the voltage is turned on in both cases, but that of the TrPeLED without the SnO_x is approximately 2 orders of magnitude higher than the corresponding devices that contain the SnO_x layer. This increase in current density is due to shunt paths, that lead to a large leakage current (Figure S5).

Figure 1b also illustrates the dependence of the light emission on the voltage. Since light-emission occurs on both sides, from now on we define the emission from the substrate side as the bottom emission and that from the SnO_x/ITO side as the top emission. If not specified, the reported luminance and efficiency values will refer to the combined values. The relevant performance figures of merits for the devices are summarized in Table S4. Since the large leakage currents make it difficult to pinpoint the minimum voltage needed to inject carriers, we define the turn-on voltage as the voltage at which the luminance is equal to 20 cd m^{-2}. In short, the devices incorporating the SnO_x buffer layer turned on at a low voltage of 2.8 V, which is indicative of efficient carrier injection, and then reached a peak luminance of 90 000 cd m^{-2} at 6 V, while their efficiency was just short of 4%. On the contrary, the devices without the protective SnO_x buffer layer had a peak luminance less than 9000 cd m^{-2} and a maximum EQE of only 0.18%. We note that the SnO_x-free devices had a high current density in the 0–2.5 V range indicative of shunts [35]. These findings demonstrate the vulnerability of thin organic transport layers and perovskite active layers in PeLEDs to plasma damage from the ITO deposition process, as well as the possibility of SnO_x to partially mitigate the limitations of TCOs fabrication via sputtering.

Compared to the opaque LEDs with the same active stack but employing a Ba/Ag top electrode (Figure S6), the TrPeLEDs had a significantly higher leakage current even when the SnO_x layer was employed. This implies that magnetron sputtering for the TCO does not lead to very good devices. We, therefore, explored pulsed laser deposition (PLD) as an alternative method for the TCO deposition. PLD allows higher chamber pressures than sputtering, enabling more efficient thermalization of energetic particles, which is advantageous for damage mitigation [42], as demonstrated in perovskite solar cells [43]. Besides the method of ITO deposition we kept the device stack the same and refer to it as devices "***1c***". Details on the deposition conditions via PLD can be found in the Experimental Section. The work function of the PLD-deposited ITO film (4.70 eV, as shown in the energy diagram, Figure S3) was experimentally determined by contact potential difference (CPD) (Figure S7).

The current density versus voltage of these ***1c*** type devices is shown in Figure 2a. After a steep rise, a plateau appears up to 3 volts, after which the current density further increases typical for diode-like behavior. In the devices without the SnO_x layer, a higher initial current density is observed. Compared with type ***1a*** and ***1b*** devices the current density of device ***1c*** is lower, whereas the luminance reaches similar levels. The bottom emission is more intense and reaches a maximum luminance above 80 000 cd m^{-2} at a driving voltage of 6.0 V, while the top emission has a luminance of 68 000 cd m^{-2} at the same voltage (Figure 2b, corresponding to a bottom/top emission ratio of 1.18). The combined luminescence (148 000 cd m^{-2}) is thus similar as in type ***1a*** and ***1b*** devices. The decrease in current density is thus the reason for the increase in EQE of the ***1c*** type devices (Figure 2c). A maximum EQE of 11% is obtained whereas the average is 5.3% across 43 devices, (Figure S8), which shows that the current density fluctuates from batch to batch indicating that further improvement is needed. Nevertheless, the PLD-based ITO in combination with SnO_x allows for the forming of diodes with limited leakage currents and high-efficiency electroluminescence. The electroluminescence (EL) spectra of the obtained devices, measured from the substrate side, is shown in Figure 2d. It is slightly blue shifted compared to the photoluminescence (PL) spectrum of the perovskite layer (Figure S9a), which may be due to a small reduction in the excited state energy under the influence of the applied field [44]. It overlaps with that of the opaque device fabricated for reference purposes (Figure S9b), showing that the use of a transparent electrode does not affect the shape or the position of the light emission. The emission spectrum was also acquired from the top side of the devices (Figure S9c) and at different voltage values (Figure S9d), and no appreciable differences were found. Optical simulations for the two types of electrodes (Figure S10a) or for the two directions of observation (Figure S10b) confirm the weak influence of the cavity. The narrow peak (full width at half maximum, FWHM, of 22 nm) translates to a bright, pure yellowish green emission (photo of a device in its on state in Figure 2e), as also confirmed by the near-edge position of the corresponding color point in the International Commission on Illumination (CIE) chromaticity diagram (Figure 2f).

The dependence of the luminescence on the emission direction (top vs bottom) most likely does not originate from an anisotropic

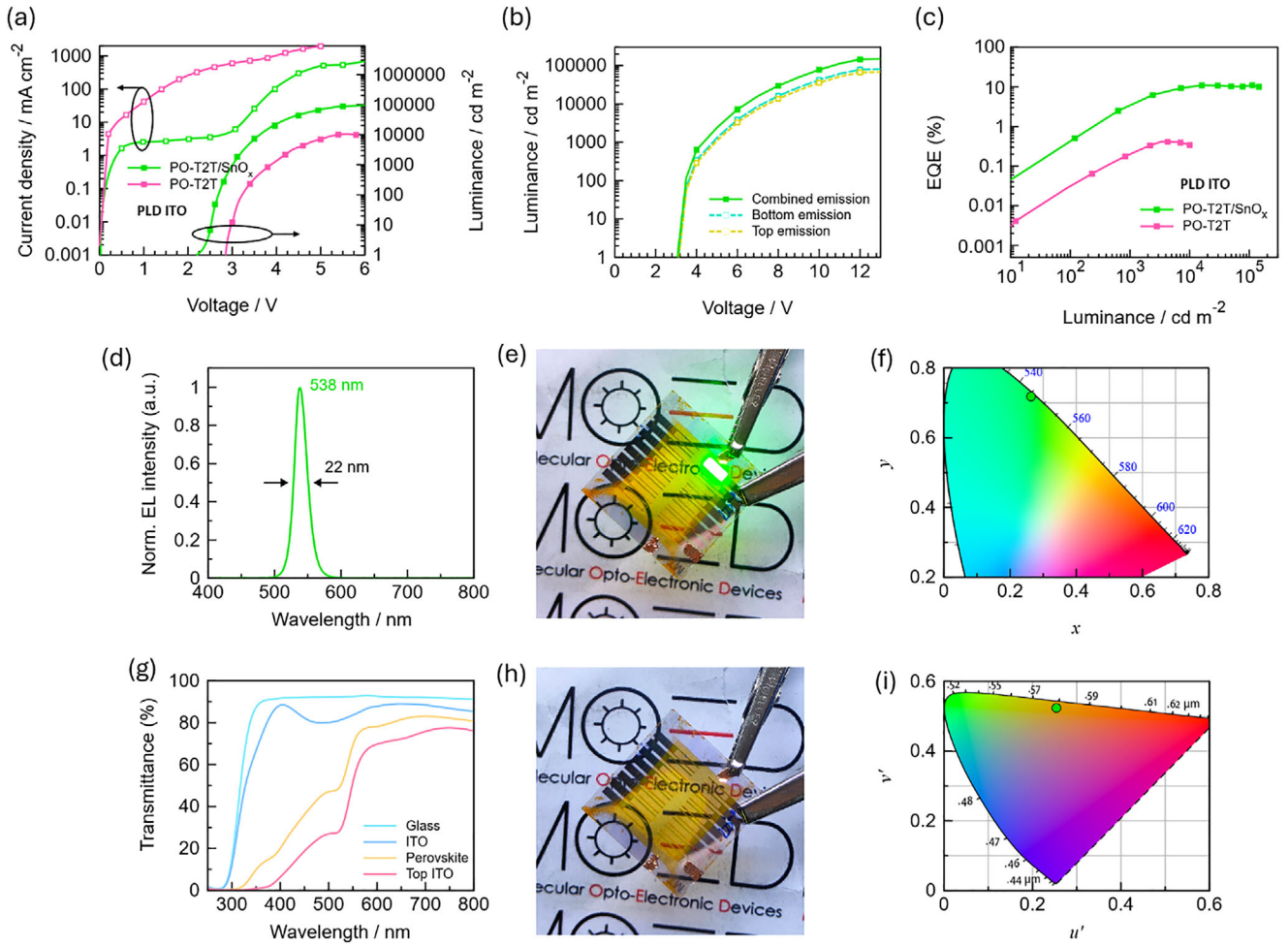

FIGURE 2 | Characterization of the TrPeLEDs with p-type in situ NCs and an ITO cathode deposited through pulsed laser deposition. (a) Current density and combined luminance *vs* voltage curves for devices with or without the buffer SnO_x layer (devices "1c" and "1d"). (b) Luminance *vs* voltage curves showing the light emitted from either side of the device and the total emitted light. (c) Efficiency *vs* luminance plot for the same devices. (d) EL spectrum measured from the bottom side (devices "1c"). (e) Photo of the bottom side of a device turned on. (f) Corresponding point in the CIE 1931 *xy* chromaticity diagram. (g) Transmittance spectrum of the device stack "1c" after the deposition of each layer. The legend in the plot denotes the last layer deposited before the transmittance measurement. (h) Photo of the bottom side of a "1c" device on a white background with text. (i) Corresponding point in the CIE 1976 uniform chromaticity scale (UCS) diagram.

emission. Optical simulations of the device stack assuming isotropic emission and taking into account parasitic absorption and optical interference effects due to the refractive index mismatch between each layer accurately predict the experimentally observed emission ratio (Figure S11). The effect of the different layers in the stack on the transmittance can be seen in Figure 2g [45]. In addition, the simulations hint at the possibility to tune the relative amount of light emitted in the two directions, by varying the electrodes' thickness.

While the efficiency value observed for device type ***1c*** is similar with that of the best-performing TrPeLEDs based on DMD type top cathodes (Table S1), the maximum luminance is more than one order of magnitude higher (see Figure 4c). This is thanks to the combination of two factors. On the one hand, to the ultrahigh peak brightness of these devices with an in situ NCs EML, whose excellent charge-transport characteristics are not impeded by organic ligands [26]. On the other hand, to the transparent electrode deposition strategy, which preserves the intrinsic high-luminance properties of the device. This was corroborated by the fabrication of devices with the same intrinsically bright emissive layer but with a DMD top cathode of MoO_x (10 nm)/Au (7 nm)/MoO_x (5 nm) (Figure S12). These devices reached a much lower luminance (232 cd m^{-2} at 8.7 V), a lower maximum efficiency (0.86% at 9.52 cd m^{-2}) as well as a more unbalanced bottom/top emission ratio (2.66).

The TrPeLED is slightly less efficient than the opaque counterpart (Figure S6b) [28], indicating some degree of photon loss in the TrPeLEDs. In previous reports of TrPeLEDs, such losses have been attributed to a more difficult charge injection from the higher work function transparent top contact electrode (ITO compared to Ba). This is most likely the reason for the slightly higher turn-on voltage value. Optical simulations also show that changing the thickness of either of the two electrodes would lead to a higher total radiance (Figure S13). This indicates that some losses are also related to a high fraction of generated light being coupled into waveguided modes and trapped within

the stack [35]. The lifetime of the transparent devices was also assessed. Upon driving them with a constant current density corresponding to an initial combined luminance value of 190 cd m^{-2}, conditions under which it took 4.0 min for the luminance to reach half its initial value (T50) (Figure S14). Additional lifetime measurements applying higher initial luminances were also assessed (Figure S15). The obtained lifetime values, albeit comparable to other previously described TrPeLEDs [35], is lower to that of the corresponding opaque counterpart reported in literature [28]. This suggests that the degradation is not caused by the decomposition of the perovskite, or creation of new non-radiative traps in the emissive layer. But rather that the most plausible routes of degradation are related to interfacial or electrode degradation. This was confirmed by measuring the PL and taking SEM images before and after the lifetime test. There was a negligible decrease in the intensity of the PL spectrum (Figure S16a) and the SEM images showed no significant changes in the morphology of the film (Figures S4 and S16b for pristine and biased device, respectively).

The softer TCO deposition of PLD compared to magnetron sputtering, which is responsible for the remarkable increase in performances of the transparent devices, questions the need for a protective layer prior to the TCO deposition. To check this, PLD ITO was also deposited directly on top of the ETL, as is common practice with opaque metal cathodes (devices "**1d**"). The TrPeLEDs turned on at a slightly higher turn-on voltage of 2.85 V, yet they only reached a combined emission of 10 000 cd m^{-2} and a maximum EQE of 0.416% (Figure 2a,c). This counter experiment demonstrates that also for PLD-based TCO deposition the TrPeLEDs improve when a protective buffer layer is employed.

To enable their integration in practical applications (e.g. lighting panels, see-through displays or in architectural window glass), the appearance of TrLEDs is just as important as their luminance and EQE. The first metric to consider is the transmittance, that is, the fraction of incident light that passes through them rather than being reflected or absorbed. The figures of merit that are usually reported are the average transmittance in the visible range (400–700 nm), the maximum and minimum value in that wavelength range and/or the value at the maximum wavelength of emission. For our devices, the transmittance varied considerably from 6.5% at 400 nm to 75.9% at 700 nm, resulting in an average value of 46.7% (Figure 2g). The value is slightly higher than the devices prepared with a DMD top cathode (44.6%, Figure S17). At the maximum wavelength of the emission (538 nm), the transmittance was 35.3%. However, the average value does not always reflect how transparent the devices appear to the human eye. This is because our eyes perceive green light brighter than red or blue light of the same intensity. In addition, the light coming from the sun or from artificial light sources is not equally intense at all wavelengths. The calculation of the so-called average visible transmittance (AVT) takes both the photopic response function and the spectral power distribution of the light source into account and thus yields a more meaningful figure of merit [46]. The most fitting usage scenario for our type ***1c*** TrPeLEDs in view of their remarkably high luminance, is for outdoor applications. For this application scenario the reference terrestrial solar spectral irradiance spectrum or the D series of published CIE illuminants that represent natural daylight are recommended to be used in the colorimetric calculations by the CIE [47]. The AVT of the devices of this work, calculated with the CIE standard illuminant D65 is 50.9%. This is higher than the average transmittance value (46.7%). This is caused by the high device absorption in the blue region of the spectrum, which reduces the average transmission. This is, however, neither intense in the natural daylight spectrum nor is the human eye sensitive in that region.

On the other hand, the transparency alone is not enough to evaluate the aesthetic quality. The transmittance spectrum is almost never flat through the visible spectrum, the color of objects behind the transparent devices will appear differently as compared to objects under natural daylight. The fidelity with which colors are reproduced is quantitatively evaluated by the color rendering index (CRI), the CIELAB color coordinates (a^*, b^*), and the CIE 1976 UCS color space coordinates (u', v'). Our type ***1c*** TrPeLEDs have an unequal transmittance throughout the visible spectrum (Figure 2g). This leads to a low CRI of 44.87, and (u', v') coordinates of (0.24, 0.52, Figure 2i) and (a^*, b^*) coordinates of (14.5, 43.8) that indicate a reddish-yellowish tint (Figure 2h; Table S3). Despite this tint, the very high brightness and the haze-free appearance still ensure a very high on/off contrast from both the bottom and the top side (Figure S18).

2.2 | Tuning of the Emissive Layer Thickness

Despite their good emission properties, the unsatisfactory aesthetic quality of our type ***1c*** TrPeLEDs motivated the search for strategies to improve it. Both transmittance measurements (Figure 2g) and optical simulations (Figure S19) show that the perovskite film is responsible for most of the light absorption in the visible range. This means that improvements of the overall device transmittance and aesthetic quality can only come from a reduction in the thickness of the emissive layer. Hence, we fabricated transparent PeLEDs with the same architecture but with thinner perovskite layers (half of the thickness used in device type ***1c***). These thinner devices are referred to as device type "***1e***" (details in the Experimental section). The resulting devices appear considerably more transparent (Figure 3a), as confirmed by the transmittance spectrum (Figure 3b) and by the AVT value (66.4%, compared to 50.9%). This AVT is approaching the value that is generally accepted for automotive applications. As expected, the highest increase in transmittance was recorded above the perovskite bandgap (< 550 nm). The consequent improvement in the shape of the transmission spectrum enhances the color fidelity. This leads to a higher CRI value (89.2 vs 44.9) and lower (a^*, b^*) coordinates (Table S3), which result in a pale yellowish-white tint (Figure 3c) and in an even larger on/off contrast when the devices are operated (Figure 3d).

The reduction by a factor two in thickness is beneficial not only for the aesthetic properties of the devices but also for the turn-on voltage, which decreased from 3.03 to 2.53 V (Figure S20a). However, both the maximum luminance and the peak efficiency are lower (19 182 cd m^{-2} at 6.3 V and 1.48%, respectively, Figure S20b). This is due to a more pronounced quenching of the emission in devices due to a reduced emission area (also observed in opaque devices Figure S21) and to a reduced light outcoupling (Figure S22). Hence, the device transmittance, luminance, and

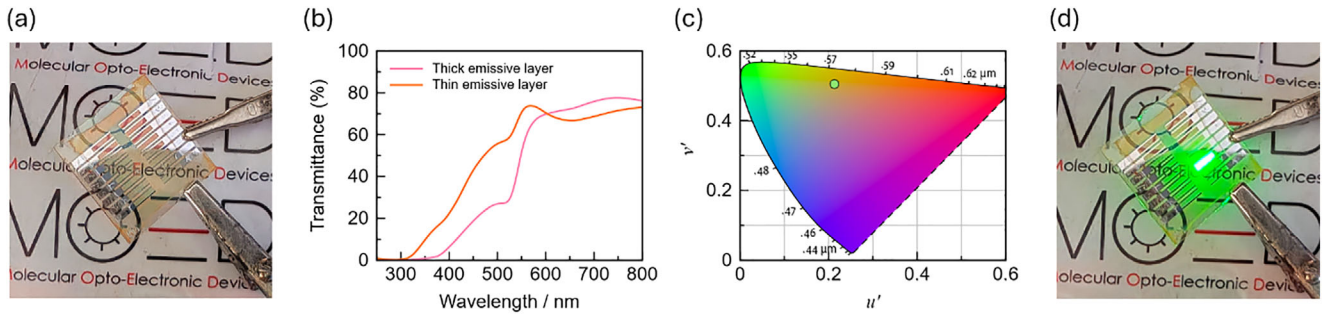

FIGURE 3 | TrPeLEDs with a thinner layer of p-type in situ NCs. (a) Top side of TrPeLEDs in the off state. (b) Transmittance spectrum of the full devices ("1e") compared to that of reference TrPeLEDs with a thicker emissive layer ("1c"). (c) Corresponding point in the CIE 1976 uniform chromaticity scale diagram. (d) Top side of TrPeLEDs in the on state.

efficiency can be altered through the perovskite thickness allowing the address specific application. Optical simulations were also performed to predict in detail how the transmittance changes with the thickness of the perovskite (Figure S23a) and the ITO electrodes (Figure S23b).

2.3 | Application to Other Perovskite and Device Structures

Metal halide perovskites have a large compositional parameter space allowing for structure property optimizations. However, this variability in compositions makes it difficult to develop a universal device architecture suitable for all the possible perovskite structures. Nevertheless, the soft cathode deposition detailed above does lend universality to our approach to transparent LEDs. To demonstrate this, we fabricated TrPeLEDs with two additional perovskite structures and with different ETLs.

First, we fabricated TrPeLEDs using an EML based on a core/shell perovskite NCs, which were obtained via the in situ reaction of benzylphosphonic acid (BPA) with a polycrystalline perovskite film (average size of 10 ± 2 nm, obtained by SEM and TEM images, Figure S24) that are referred to as device type ***2a*** [26]. These TrPeLEDs had the following architecture; ITO (160 nm)/GraHIL (75 nm)/EML (280 nm)/ 2-[4-(9,10-di-naphthalen-2-yl-anthracen-2-yl)-phenyl]-1-phenyl-1H-benzoimidazole (ZADN; 45 nm)/tin oxide (SnO_x; 20 nm)/ITO (100 nm) (device type ***2a″***, cross-sectional SEM image in Figure S25). In summary, the perovskite thin films were deposited on a hole-injection layer with a gradient work function (GraHIL). They were exposed to a BPA containing solution, which can penetrate and intercalate into the large perovskite crystals, forming the small grains (for more details, refer to the Experimental section). After the vacuum deposition of the ZADN ETL on top of the EML, SnO_x and ITO were deposited using ALD and PLD methods, respectively, as previously described. Despite the additional hole injection layer, the resulting TrPeLEDs have a similar AVT (54.7%, Figure S26a and Table S3) as device type ***1c*** and no haze. This is due to the high transmittance of PEDOT:PSS in the visible region. Therefore, text or image positioned behind these TrPeLEDs remains readable (Figure S27), albeit with the same yellow tint as seen for the type ***1c*** TrPeLED ($CIEL_{u'v'}$ = (0.24, 0.54), Figure S26b). Their EL spectrum (Figure S28a), measured from the bottom electrode, shows a green narrowband emission (λ_{max} = 539 nm, FWHM = 21 nm, $CIE_{x,y}$ = 0.26, 0.72, Figure S28b and Table S2), almost superimposable with the PL spectrum of the in situ core/shell PeNCs films (Figure S28c). This is identical to that of opaque devices using the same emissive layer stack but using a thick metal cathode and is independent of the side of observation and the voltage applied (Figure S28d–f). The electroluminescence is visible starting from 6.23 V (Figure S29a), a value higher than for the type ***1*** devices. The difference could be a consequence of an increased barrier for electron injection from SnO_x into the ETL, as ZADN has a substantially shallower LUMO energy (−2.90 eV) when compared to PO-T2T (−3.22 eV) and SnO_x (−4.36 eV, Figure S30). This also limits the maximum external quantum efficiency of the devices (EQE_{max} = 1.28%, Figure S29b) and the maximum combined luminance (14 929 cd m^{-2}). Control devices, type ***2b***, were prepared without the protective SnOx layer and using sputtering for the ITO deposition. In these type ***2b*** TrPeLEDs the turn-on voltage is reduces with respect to type ***2a*** devices (Figure S31a) possibly related to the smaller overall device thickness. However, the maximum luminance (1070 cd m^{-2}) and efficiency (0.07%, Figure S31b) are lower. This confirms that direct sputtering of ITO on these LEDs induces damage in the EML or ETL.

The PeNCs that were formed in-situ during film formation can also be synthesized prior to the layer deposition leading to a PeNC suspension. These PeNC suspensions can then be spin-coated to form a homogeneous film. However, as the PeNC concentration is low in these suspencions, a limit imposed by the colloidal stability, the resulting films tend to be thin. This is beneficial for transparent devices as these thin films have a high light transmission but may lead to more shunt paths. We prepared TrPeLEDs based on colloidally synthesized $FA_{0.9}GA_{0.1}PbBr_3$ nanocrystal structures, type ***3c***. These TrPeLEDs had the following architecture; ITO (160 nm)/GraHIL (75 nm)/ colloidal NCs film / 1,3,5-tris(1-phenyl-1H-benzimidazol-2-yl)benzene (TPBi) (the architecture and cross-sectional SEM image of this ***3c*** device type are illustrated in Figure S32). The use of cation alloying in the PeNC generates smaller particles [24], which confines electrons and holes and boosts the radiative recombination (average size of 9.82 ± 0.22 nm, TEM image of the NCs in Figure S33). While TPBi adsorbs onto the perovskite surface, reduces the nonradiative recombination and improves the photoluminescence quantum yield of the PeNCs films [25]. As expected, the type ***3a*** devices were very transparent. Text or image positioned behind these TrPeLEDs could be perfectly observed

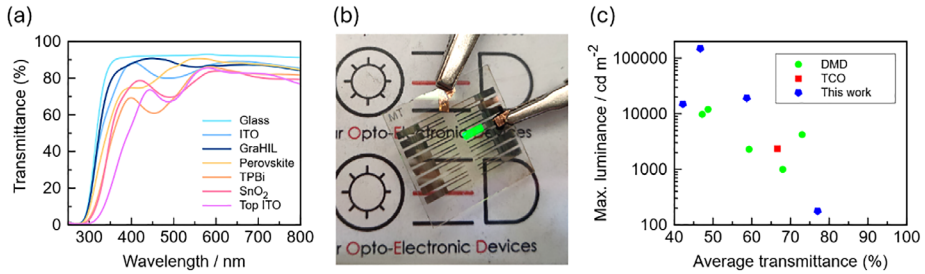

FIGURE 4 | Transparent PeLEDs based on colloidal NCs. (a) Transmittance spectrum of the device stack ("*3a*") after the deposition of each layer. The legend in the plot denotes the last layer deposited before the transmittance measurement. (b) Photo of the bottom side of a device turned on. (c) Comprehensive summary of all reported TrPeLEDs characteristics on the basis of maximum luminance and average transmittance, categorized according to their cathode material, available in the literature to date. Ref: [31, 33–38]. For NIR-emitting devices, a fictitious maximum luminance value that assumes emission at 538 nm and a luminous efficacy equal to that of the TrPeLEDs in this work (655.71 lm W^{-1}) was used for comparison.

without any distortions, haze or blurring and with only minimal luminosity or color altering (Figure 4b; Figure S34). These type ***3a*** TrPeLEDs have an AVT of around 80% (Figure 4a; Table S3), which represents, to the best of our knowledge, the highest value for TrPeLEDs (Figure 4c), and a very high CRI value above 90. At the same time, the near-the-origin values for a^* and b^* indicate an almost neutral color (Figure S35).

Similarly, to type ***2*** devices (with in situ core/shell PeNCs), devices of type ***3*** (with colloidal PeNCs) have a relatively high turn-on voltage of 8.64 V (Table S4), possibly due to the same misalignment between the conduction band of SnO_x and the LUMO of the employed ETL (TPBi, Figure S36). The electroluminescence is centered at a slightly lower wavelength of 530 nm (Figure S37a). This, together with a small FWHM value of 21 nm is indicative of monodispersed particles. This results in a CIE-y value of >0.79 (Figure S37b) required for the green primary color in the ITU-R Recommendation BT.2020 (Rec. 2020) standard suggested for ultra-high-definition vivid displays [48]. Analogously to the previously described devices, their emission overlaps with the PL spectrum of the film and is independent of the viewing direction, the cathode and of the voltage applied (Figure S37c–f). Finally, a voltage scan was performed until 20 V, at which the devices reached a luminance of 178.22 cd m^{-2} and an EQE slightly short of 0.1% (Figure S38). These relatively low values are caused mainly by the low current densities, likely due the insulating characteristics of the organic ligands that can impede charge injection and transport [49, 50]. The leakage current is not very high, indicating that the damage of the TCO deposition is not the main problem, which is interesting in view of the thin emitting layer.

Together, these findings confirm that our approach to fabricate transparent PeLEDs is applicable to a wide range of device architectures employing different perovskite-based EMLs.

3 | Conclusion

In conclusion, in this work, we showed how a combination of ALD and PLD, both scalable techniques, can be used to prepare highly luminescent perovskite light-emitting diodes with a high transmission. Three different types of perovskite based emitters were evaluated in transparent LED structures. The LEDs were thoroughly characterized from both an electrical and optical point of view. The qualities of the transparent conductive oxides as well as the damage mitigation strategies employed enabled the demonstration of both the brightest (~150 000 cd m^{-2}) and the most transparent (AVT ≈ 80%) perovskite LEDs. These LEDs could cover a range of potential applications from see-through displays and lighting panels to smart windows, walls, and doors.

4 | Experimental Section

4.1 | Materials

Lead bromide ($PbBr_2$, >99.999%), formamidinium bromide (FABr, >99.5%), (4-(3,6-dibromo-9H-carbazol-9-yl)butyl)phosphonic acid (4PACz, >99%), 1,3,5-tris(1-phenyl-1-H-benzimidazol-2-yl) benzene (TPBi, >99.8%) and 2,4,6-tris[3-(diphenylphosphinyl) phenyl]-1,3,5-triazine (PO-T2T, >99%) were purchased from Lumtec. Cesium bromide (CsBr, >99.999%) and anhydrous toluene (99.8%) were purchased from Alfa Aesar. Methylammonium bromide (MABr, >99.99%) was purchased from Greatcellsolar. Guanidinium bromide (GABr, >98%), chloroform ($CHCl_3$, ≥99%), toluene (≥99.5%), 1-butanol (99.8%), oleic acid (OA, 90%), decylamine (≥99.0%), chlorobenzene (99.8%), tetrahydrofuran (THF, ≥99.9%) and dimethyl sulfoxide (DMSO, ≥99.5%) were purchased from Sigma–Aldrich. Benzylphosphonic acid (BPA, 97%) was purchased from Thermo Scientific Chemicals. Poly(3,4-ethylenedioxythiophene) polystyrene sulfonate (PEDOT:PSS Clevios P VP AL 4083) was purchased from Heraeus. 2-[1-[difluoro[(trifluoroethenyl)oxy]methyl]-1,2,2,2-tetrafluoroethoxy]-1,1,2,2-tetrafluoroethanesulfonic acid (Nafion Dispersion Solution, 5%, DE520 CS type) was purchased from Fujifilm. ZADN (2-[4-(9,10-Di-naphthalen-2-yl-anthracen-2-yl)-phenyl]-1-phenyl-1H-benzoimidazole, >99%) was purchased from Ossila. All materials were used as received without further purification.

4.2 | p-Type in Situ NCs-Based Devices Fabrication

For devices "1", pre-patterned 160 nm thick indium tin oxide (ITO)-coated glass plates (3 cm × 3 cm) were used as transparent

conductive substrates. They were subsequently cleaned ultrasonically in tap water-detergent, deionized water, and 2-propanol baths for 5 min. After drying, the substrates were placed in a UV–ozone cleaner (Jelight 42–220) for 20 min. The substrates were transferred to a glovebox with water and oxygen concentrations below 10 ppm for the deposition of the emissive layer.

A precursor solution, prepared by dissolving FABr, MABr, GABr, CsBr, $PbBr_2$, and 4PACz at a molar ratio of 0.8:0.1:0.1:0.15:1:0.05 in dimethyl sulfoxide, was pre-spun at 500 rpm for 10 s and then spin-cast at 5000 rpm for 90 s. The concentration was 0.95 mol l^{-1} for devices with a thick layer (1a-d) and 0.425 mol l^{-1} for devices with a thin layer (1e). 100 µl of a 2 mg mL^{-1} TPBI solution in chloroform were dripped after 40 s during the second step. Then, the samples were annealed at 90°C for 10 min. The substrates were transferred to a thermal evaporator where PO-T2T was deposited at a vacuum evaporation rate of 0.06 nm s^{-1}.

4.3 | In Situ Core/Shell Perovskite NCs-Based Devices Fabrication

For devices "2", the same pre-patterned ITO-coated glass plates were cleaned and placed in a UV–ozone cleaner, like described above. Then, a PEDOT:PSS / Nafion dispersion mixture with a 1:1 weight ratio was spin coated to form a 75 nm-thick hole-injection layer (GraHIL). The layer was annealed at 150°C for 30 min, and the substrates were transferred to a glovebox. The active layer precursor solution, prepared by dissolving FABr, MABr, GABr, CsBr, $PbBr_2$, and BPA at a molar ratio of 0.7:0.1:0.2:0.15:1:0.1 in dimethyl sulfoxide with a concentration of 1.20 mol l^{-1}, stirring it overnight in an N_2-filled glovebox at room temperature and filtering it using 0.22 µm polytetrafluoroethylene filters, was spin-cast at 6000 rpm for 90 s. During the spinning step, a 2 mg mL^{-1} TPBi solution in chlorobenzene was dropped onto the spinning film after 60 s. Then, a 3 mg mL^{-1} BPA solution in THF was loaded on top of the perovskite, followed by a reaction time of 30 s and direct spin drying afterward. Finally, the samples were annealed at 70°C for 10 min and transferred to a thermal evaporator where ZADN was deposited at a vacuum evaporation rate of 0.06 nm s^{-1}.

4.4 | Colloidal PeNCs-Based Devices Fabrication

For devices "3", the same pre-patterned ITO-coated glass plates were cleaned, placed in a UV–ozone cleaner, and coated with a GraHIL like described above. Before continuing, $FA_{0.9}GA_{0.1}PbBr_3$ PeNCs were prepared by ligand-assisted reprecipitation (LARP) method. The precursor solution was prepared by dissolving FABr (0.18 mmol), GABr (0.02 mmol), and $PbBr_2$ (0.1 mmol) in 0.5 mL of N,N-dimethylformamide (DMF). The mixture of the non-polar solvent and ligands for reprecipitation was composed of toluene (5 mL), 1-butanol (2 mL), OA (300 µl), and DAm (24.2 µl). The precursor solution (0.15 mL) was dropped into the non-polar solvent mixture under vigorous stirring. After 10 min, colloidal PeNCs were washed by sequential centrifugation and dispersed in anhydrous toluene. Finally, the PeNCs-dispersed toluene solution was mixed with a TPBi solution in toluene (5 mM) with a volume ratio of 10:1. At this point, the GraHIL-coated substrates were transferred to a glovebox, where the PeNCs-dispersed toluene solution mixed with TPBi was spin-coated on the substrates at 500 rpm for 60 s to form PeNCs films. The samples were then transferred to a thermal evaporator where TPBi was deposited at a vacuum evaporation rate of 0.06 nm s^{-1}.

4.5 | Cathode Deposition

For opaque reference devices, Ba (3 nm) and Ag (100 nm) were sequentially evaporated on top of the ETL at a rate of 0.2 nm s^{-1}, with the background pressure being around 10^{-6} mbar. For transparent devices, a 20 nm layer of SnO_x was deposited by ALD using an Arradiance's GEMStar XT Thermal ALD system integrated into a nitrogen-filled glovebox following a procedure recently published by us [51]. Then, the ITO films were deposited at room temperature either using a using a Solmates large-area PLD 200 mm system or an Amstrong DC magnetron sputtering deposition equipment, both coupled to a N_2 glovebox. In the former case, a Lightmachinery's IPEX-700 KrF excimer laser (λ = 248 nm) was employed, setting the repetition rate at 50 Hz and the fluence at 1.5–1.6 J cm^{-2}. The source material for ITO deposition was a SnO_2:In_2O_3 ceramic target with 2:98 wt.%, acquired from Pi-kem, and the chamber pressure was set at 0.033 mbar, with an O_2 partial pressure of 0.007 mbar controlled by a constant injection of an oxygen/argon gas mix, as optimized in our previous paper [41]. In the latter case, the system was equipped with a TRUMPF Huettinger pulsed DC power supply (2.0 kW, 0–100 kHz, 0–800 V, 0–5 A) and a circular sputtering target with a composition of SnO_2:In_2O_3 (97%:3%), a diameter of 4 inches, and a purity of 99.99%. The pressure was 0.005 mbar, the power 500 W and the carrier gas Ar (with a flow of 20 sccm). In either case, the ITO was deposited through shadow masks to ensure a final active area of 8.25 mm^2 as defined by the overlap of the bottom and top electrode. The devices were finished with thermally evaporated Ag grids (100 nm thick) at the side of the top ITO electrode to reduce the resistance. Devices were not exposed to water vapor or O_2 after the cathode deposition and before the characterization.

4.6 | Structural Characterization

The SEM images were acquired with a S8010 ultra high-resolution scanning electron microscope (Hitachi High-Tech Corporation).

4.7 | Photophysical Measurements

The photoluminescence spectra of the deposited films were measured with an Avantes AvaSpec-2048L spectrometer equipped with a diode laser of integrated optics with an emission wavelength of 375 nm. The transmittance spectra were measured with the same spectrometer equipped with an Avantes AvaLight-DS-S-BAL deuterium halogen light source and optic fibers. To determine the VBM of the perovskite film, photoelectron spectroscopy analysis in air (PESA) was conducted using an APS02 ambient pressure photoemission spectroscopy (APS) system (KP Technology Ltd). For that, we used a 150 nm–thick film deposited onto a glass substrate fully coated with ITO. The system was equipped with a digital TFT oscilloscope, a 2 mm gold tip, and a 450 mm × 450 mm optical and Faraday enclosure that also allowed for the determination of the work function of the PLD ITO film.

4.8 | PeLEDs Characterization

After full device fabrication, the samples were introduced into a custom setup for a current density and luminance versus voltage (*J-V-L*) scan. For this we employed a Keithley 2400 Source-Meter and a Hamamatsu Photonics S1337-21 Si photodiode coupled to a Keithley 6485 picoammeter. For transparent devices, the bottom and top emission were measured sequentially with the same photodiode by flipping the devices. A LabVIEW program was used to control the Keithleys and to obtain the data. The photodiode was calibrated using a Konica Minolta LS-150 equipped with a 110 close-up lens for the measurement of small areas and controlled through the CS-S20 Data Management Software. For the EQE calculations, Lambertian emission was assumed. The electroluminescence spectra were measured with an Avantes AvaSpec-2048L spectrometer and the Keithley 2400 Source-Meter.

4.9 | PeLEDs Optical Simulations

The emission simulations for the devices were obtained by simulating the full device stack with the electro-optical simulation software Setfos 5.5 (FLUXiM). In this work, only the optical characteristics were modeled, while the electronic processes were neglected. For simplicity, the spatial distribution of the emitter molecules was assumed to be gaussian, with the peak located at the center of the emitter layer (relative position = 0.5) with a width of 50 nm. The refractive index (n, k) values used in the simulation were sourced from literature [26]. For the p-type in situ NCs film and for glass, a constant n value of 2.15 and 1.5 were employed, respectively.

5 | Statistical Analysis

Statistical analyses were performed using OriginLab Corporation's Origin 9 and Microsoft Excel. Prior to analysis, the data were inspected for consistency and reproducibility across independently fabricated devices. For each device architecture or material composition, at least 16 devices were analyzed to evaluate reproducibility and overall performance trends. The electrical and optical characteristics reported in the main figures correspond to the best-performing devices; however, these devices were selected only after confirming that their behavior was representative of the general properties observed across the full set of analyzed devices. No additional data transformation was applied unless explicitly stated. When computing average values, outliers were not excluded unless clearly attributable to experimental artifacts.

Acknowledgements

This project has received funding from the European Union Horizon 2021 research and innovation programme under grant agreement No. 101073045 (TADFsolutions) and by the State Secretariat for Telecommunications and Digital Infrastructure, from the Ministry of Economic Affairs and Digital Transformation in the framework of the European Recovery, Transformation and Resilience Plan, with funding from European Union NextGenerationEU, project nr: TSI-069100-2023-0012- PERTE chip and from the Ministry of Science and Innovation (MCIN) and the Spanish State Research Agency (AEI): project PID2024-159087OB-I00 funded by MICIU/AEI/10.13039/501100011033″ and "ERDF A way of making Europe". T.W. Lee acknowledges the National Research Foundation of Korea (NRF) grant funded by the Ministry of Science and ICT (MSIT) (Grant Number. RS202500560490).

Funding

This project has received funding from the European Union Horizon 2021 research and innovation programme under grant agreement No. 101073045 (TADFsolutions) and by the State Secretariat for Telecommunications and Digital Infrastructure, from the Ministry of Economic Affairs and Digital Transformation in the framework of the European Recovery, Transformation and Resilience Plan, with funding from European Union NextGenerationEU, project nr: TSI-069100-2023-0012- PERTE chip and from the Ministry of Science and Innovation (MCIN) and the Spanish State Research Agency (AEI): project PID2024-159087OB-I00 funded by MICIU/AEI/10.13039/501100011033″ and "ERDF A way of making Europe". T.W. Lee acknowledges the National Research Foundation of Korea (NRF) grant funded by the Ministry of Science and ICT (MSIT) (Grant Number. RS202500560490).

Conflicts of Interest

The authors declare no conflicts of interest.

Data Availability Statement

The data that support the findings of this study are available from the corresponding author upon reasonable request.

References

1. X. Hong, T. Ishihara, and A. V. Nurmikko, "Photoconductivity and Electroluminescence in Lead Iodide Based Natural Quantum Well Structures," *Solid State Communications* 84 (1992): 657–661, https://doi.org/10.1016/0038-1098(92)90210-Z.

2. K. Chondroudis and D. B. Mitzi, "Electroluminescence From an Organic–Inorganic Perovskite Incorporating a Quaterthiophene Dye Within Lead Halide Perovskite Layers," *Chemistry of Materials* 11 (1999): 3028–3030, https://doi.org/10.1021/cm990561t.

3. Z.-K. Tan, R. S. Moghaddam, M. L. Lai, et al., "Bright Light-Emitting Diodes Based on Organometal Halide Perovskite," *Nature Nanotechnology* 9 (2014): 687–692, https://doi.org/10.1038/nnano.2014.149.

4. Y.-H. Kim, H. Cho, J. H. Heo, et al., "Multicolored Organic/Inorganic Hybrid Perovskite Light-Emitting Diodes," *Advanced Materials* 27 (2015): 1248–1254, https://doi.org/10.1002/adma.201403751.

5. M. Li, Y. Yang, Z. Kuang, et al., "Acceleration of Radiative Recombination for Efficient Perovskite LEDs," *Nature* 630 (2024): 631–635, https://doi.org/10.1038/s41586-024-07460-7.

6. S.-C. Feng, Y. Shen, X.-M. Hu, et al., "Efficient and Stable Red Perovskite Light-Emitting Diodes via Thermodynamic Crystallization Control," *Advanced Materials* 36 (2024): 2410255, https://doi.org/10.1002/adma.202410255.

7. S.-Q. Sun, J.-W. Tai, W. He, et al., "Enhancing Light Outcoupling Efficiency via Anisotropic Low Refractive Index Electron Transporting Materials for Efficient Perovskite Light-Emitting Diodes," *Advanced Materials* 36 (2024): 2400421, https://doi.org/10.1002/adma.202400421.

8. Y. Gao, Q. Cai, Y. He, et al., "Highly Efficient Blue Light-Emitting Diodes Based on Mixed-Halide Perovskites With Reduced Chlorine Defects," *Science Advances* 10 (2024): ado5645, https://doi.org/10.1126/sciadv.ado5645.

9. T. Matsushima, F. Bencheikh, T. Komino, et al., "High Performance From Extraordinarily Thick Organic Light-Emitting Diodes," *Nature* 572 (2019): 502–506, https://doi.org/10.1038/s41586-019-1435-5.

10. Y. Tian, Y. Ling, Y. Shu, et al., "A Solution-Processed Organometal Halide Perovskite Hole Transport Layer for Highly Efficient Organic Light-Emitting Diodes," *Advanced Electronic Materials* 2 (2016): 1600165, https://doi.org/10.1002/aelm.201600165.

11. Y. Zhang, F.-X. Yu, X.-J. Ma, et al., "Efficient Red Phosphorescent Organic Light Emitting Diodes Based on Solution Processed All-Inorganic Cesium Lead Halide Perovskite as Hole Transporting Layer," *Organic Electronics* 50 (2017): 411–417, https://doi.org/10.1016/j.orgel.2017.08.015.

12. Y. Feng, J. Xu, H. Shan, et al., "Organometal Halide Perovskite as Hole Injection Enhancer in Organic Light-Emitting Diode," *Organic Electronics* 51 (2017): 257–263, https://doi.org/10.1016/j.orgel.2017.09.027.

13. T. Zhou, C. Liu, S. Gong, Y. Xiang, G. Xie, and C. Yang, "Boosting the Electroluminescence Efficiency of Solution-Processed Thermally Activated Delayed Fluorescence OLEDs With a Versatile Hole-Transporting Layer of Organic–Inorganic Hybrid perovskite," *Journal of Materials Chemistry C* 6 (2018): 6305–6311, https://doi.org/10.1039/C8TC01567H.

14. M. Forzatti, S.-H. Chin, M. A. Hernández-Fenollosa, M. Sessolo, D. Tordera, and H. J. Bolink, "Organic Light-Emitting Diodes Combining Thick Inorganic Perovskite Hole Transport Layers and Ultrathin Emitting Layers," *Advanced Optical Materials* 12 (2024): 2401061, https://doi.org/10.1002/adom.202401061.

15. M. Forzatti, V. Held, E. Stanzani, et al., "Organic Light-Emitting Diodes Comprising an Undoped Thermally Activated Delayed Fluorescence Emissive Layer and a Thick Inorganic Perovskite Hole Transport Layer," *ACS Photonics* 11 (2024): 4151–4160, https://doi.org/10.1021/acsphotonics.4c01039.

16. A. Fakharuddin, M. K. Gangishetty, M. Abdi-Jalebi, et al., "Perovskite Light-Emitting Diodes," *Nature Electronics* 5 (2022): 203–216, https://doi.org/10.1038/s41928-022-00745-7.

17. S.-H. Chin, D. Cortecchia, M. Forzatti, et al., "Stabilizing Single-Source Evaporated Perovskites With Organic Interlayers for Amplified Spontaneous Emission," *Advanced Optical Materials* 12 (2024): 2302701, https://doi.org/10.1002/adom.202302701.

18. O. Malinkiewicz, A. Yella, Y. H. Lee, et al., "Perovskite Solar Cells Employing Organic Charge-Transport Layers," *Nature Photonics* 8 (2014): 128–132, https://doi.org/10.1038/nphoton.2013.341.

19. A. Rogalski, F. Wang, J. Wang, P. Martyniuk, and W. Hu, "The Perovskite Optoelectronic Devices—A Look at the Future," *Small Methods* 9 (2025): 2400709, https://doi.org/10.1002/smtd.202400709.

20. S.-H. Chin, J. W. Choi, H. C. Woo, J. H. Kim, H. Seok Lee, and C.-L. Lee, "Realizing a Highly Luminescent Perovskite Thin Film by Controlling the Grain Size and Crystallinity Through Solvent Vapour Annealing," *Nanoscale* 11 (2019): 5861–5867, https://doi.org/10.1039/C8NR09947B.

21. H. Cho, S.-H. Jeong, M.-H. Park, et al., "Overcoming the Electroluminescence Efficiency Limitations of Perovskite Light-emitting Diodes," *Science* 350 (2015): 1222–1225, https://doi.org/10.1126/science.aad1818.

22. L. N. Quan, Y. Zhao, F. P. García de Arquer, et al., "Tailoring the Energy Landscape in Quasi-2D Halide Perovskites Enables Efficient Green-Light Emission," *Nano Letters* 17 (2017): 3701–3709, https://doi.org/10.1021/acs.nanolett.7b00976.

23. L. C. Schmidt, A. Pertegás, S. González-Carrero, et al., "Nontemplate Synthesis of $CH_3NH_3PbBr_3$ Perovskite Nanoparticles," *Journal of the American Chemical Society* 136 (2014): 850–853, https://doi.org/10.1021/ja4109209.

24. Y.-H. Kim, S. Kim, A. Kakekhani, et al., "Comprehensive Defect Suppression in Perovskite Nanocrystals for High-efficiency Light-emitting Diodes," *Nature Photonics* 15 (2021): 148–155, https://doi.org/10.1038/s41566-020-00732-4.

25. D.-H. Kim, S.-J. Woo, C. P. Huelmo, et al., "Surface-binding Molecular Multipods Strengthen the Halide Perovskite Lattice and Boost Luminescence," *Nature Communications* 15 (2024): 6245, https://doi.org/10.1038/s41467-024-49751-7.

26. J. S. Kim, J.-M. Heo, G.-S. Park, et al., "Ultra-bright, Efficient and Stable Perovskite Light-Emitting Diodes," *Nature* 611 (2022): 688–694, https://doi.org/10.1038/s41586-022-05304-w.

27. S. M. Park, A. Abtahi, A. M. Boehm, and K. R. Graham, "Surface Ligands for Methylammonium Lead Iodide Films: Surface Coverage, Energetics, and Photovoltaic Performance," *ACS Energy Letters* 5 (2020): 799–806, https://doi.org/10.1021/acsenergylett.0c00054.

28. W. Xiong, W. Tang, G. Zhang, et al., "Controllable p- and n-type Behaviours in Emissive Perovskite Semiconductors," *Nature* 633 (2024): 344–350, https://doi.org/10.1038/s41586-024-07792-4.

29. G. Gu, G. Parthasarathy, P. E. Burrows, et al., "Transparent Stacked Organic Light Emitting Devices. I. Design Principles and Transparent Compound Electrodes," *Journal of Applied Physics* 86 (1999): 4067–4075, https://doi.org/10.1063/1.371331.

30. G. Huseynova, J.-H. Lee, Y. H. Kim, and J. Lee, "Transparent Organic Light-Emitting Diodes: Advances, Prospects, and Challenges," *Advanced Optical Materials* 9 (2021): 2002040, https://doi.org/10.1002/adom.202002040.

31. J. Liang, X. Guo, L. Song, et al., "Transparent Perovskite Light-Emitting Diodes by Employing Organic-Inorganic Multilayer Transparent Top Electrodes," *Applied Physics Letters* 111 (2017): 213301, https://doi.org/10.1063/1.4992039.

32. E. Aydin, C. Altinkaya, Y. Smirnov, et al., "Sputtered Transparent Electrodes for Optoelectronic Devices: Induced Damage and Mitigation Strategies," *Matter* 4 (2021): 3549–3584, https://doi.org/10.1016/j.matt.2021.09.021.

33. S.-Y. Chou, R. Ma, Y. Li, et al., "Transparent Perovskite Light-Emitting Touch-Responsive Device," *ACS Nano* 11 (2017): 11368–11375, https://doi.org/10.1021/acsnano.7b05935.

34. H. Wu, Y. Zhang, X. Zhang, et al., "Fine-Tuned Multilayered Transparent Electrode for Highly Transparent Perovskite Light-Emitting Devices," *Advanced Electronic Materials* 4 (2018): 1700285, https://doi.org/10.1002/aelm.201700285.

35. C. Xie, X. Zhao, E. W. Y. Ong, and Z.-K. Tan, "Transparent Near-Infrared Perovskite Light-Emitting Diodes," *Nature Communications* 11 (2020): 4213, https://doi.org/10.1038/s41467-020-18110-7.

36. L. Cai, J. Zhou, G. Bai, et al., "High-Efficiency Top-Emitting Green Perovskite Light Emitting Diode With Quasi Lambertian Emission," *Advanced Optical Materials* 10 (2022): 2101137, https://doi.org/10.1002/adom.202101137.

37. Z. He, Z. Bao, X. Guo, et al., "Efficient Transparent Blue-emitted Perovskite Light-Emitting Diodes Based on Multilayer Transparent Top Electrodes," *Journal of Materials Chemistry C* 12 (2024): 7162–7168, https://doi.org/10.1039/D4TC00934G.

38. Y. Qi, R. Liu, Z. Li, Y. Song, C. Wang, and L. Cai, "Microcavity Forming Electrode for Efficient Color-Tunable Semitransparent Perovskite Light-Emitting Diodes," *Optics & Laser Technology* 169 (2024): 110002, https://doi.org/10.1016/j.optlastec.2023.110002.

39. L. Liu, K. Cao, S. Chen, and W. Huang, "Toward See-Through Optoelectronics: Transparent Light-Emitting Diodes and Solar Cells," *Advanced Optical Materials* 8 (2020): 2001122, https://doi.org/10.1002/adom.202001122.

40. C. Altinkaya, E. Aydin, E. Ugur, et al., "Tin Oxide Electron-Selective Layers for Efficient, Stable, and Scalable Perovskite Solar Cells," *Advanced Materials* 33 (2021): 2005504, https://doi.org/10.1002/adma.202005504.

41. K. P. S. Zanoni, A. Paliwal, M. A. Hernández-Fenollosa, P.-A. Repecaud, M. Morales-Masis, and H. J. Bolink, "ITO Top-Electrodes via Industrial-Scale PLD for Efficient Buffer-Layer-Free Semitransparent Perovskite Solar Cells," *Advanced Materials Technologies* 7 (2022): 2101747, https://doi.org/10.1002/admt.202101747.

42. Y. Smirnov, P.-A. Repecaud, L. Tutsch, et al., "Wafer-Scale Pulsed Laser Deposition of ITO for Solar Cells: Reduced Damage vs. interfacial

Resistance," *Materials Advances* 3 (2022): 3469–3478, https://doi.org/10.1039/D1MA01225H.

43. Y. Smirnov, L. Schmengler, R. Kuik, et al., "Scalable Pulsed Laser Deposition of Transparent Rear Electrode for Perovskite Solar Cells," *Advanced Materials Technologies* 6 (2021): 2000856, https://doi.org/10.1002/admt.202000856.

44. Z. Shi, Y. Li, Y. Zhang, et al., "High-Efficiency and Air-Stable Perovskite Quantum Dots Light-Emitting Diodes With an All-Inorganic Heterostructure," *Nano Letters* 17 (2017): 313–321, https://doi.org/10.1021/acs.nanolett.6b04116.

45. C. H. Park, J. G. Kim, S.-G. Jung, D. J. Lee, Y. W. Park, and B.-K. Ju, "Optical Characteristics of Refractive-Index-Matching Diffusion Layer in Organic Light-Emitting Diodes," *Scientific Reports* 9 (2019): 8690, https://doi.org/10.1038/s41598-019-45000-w.

46. C. Yang, D. Liu, M. Bates, M. C. Barr, and R. R. Lunt, "How to Accurately Report Transparent Solar Cells," *Joule* 3 (2019): 1803–1809, https://doi.org/10.1016/j.joule.2019.06.005.

47. "ISO 10526:1999/CIE S005/E-1998, CIE Standard Illuminants for Colorimetry", Geneva, Switzerland: International Organization for Standardization, 1999 n.d.

48. T.-H. Han, K. Y. Jang, Y. Dong, R. H. Friend, E. H. Sargent, and T.-W. Lee, "A Roadmap for the Commercialization of Perovskite Light Emitters," *Nature Reviews Materials* 7 (2022): 757–777, https://doi.org/10.1038/s41578-022-00459-4.

49. Y. Hassan, J. H. Park, M. L. Crawford, et al., "Ligand-Engineered Bandgap Stability in Mixed-Halide Perovskite LEDs," *Nature* 591 (2021): 72–77, https://doi.org/10.1038/s41586-021-03217-8.

50. Y. Dong, Y.-K. Wang, F. Yuan, et al., "Bipolar-Shell Resurfacing for Blue LEDs Based on Strongly Confined Perovskite Quantum Dots," *Nature Nanotechnology* 15 (2020): 668–674, https://doi.org/10.1038/s41565-020-0714-5.

51. K. P. S. Zanoni, D. Pérez-del-Rey, C. Dreessen, et al., "Tin(IV) Oxide Electron Transport Layer via Industrial-Scale Pulsed Laser Deposition for Planar Perovskite Solar Cells," *ACS Applied Materials & Interfaces* 15 (2023): 32621–32628, https://doi.org/10.1021/acsami.3c04387.

Supporting Information

Additional supporting information can be found online in the Supporting Information section.

Supporting File: adma72740-sup-0001-SuppMat.pdf.